

Kinetics of Hydrogen Absorption and Release in Zirconium Alloys During Steam Oxidation

M. Grosse · M. Steinbrueck · E. Lehmann ·
P. Vontobel

Received: 27 February 2008 / Revised: 9 June 2008 / Published online: 12 July 2008
© Springer Science+Business Media, LLC 2008

Abstract The kinetics of hydrogen absorption during steam oxidation in Zr–Sn and Zr–Nb alloys in the temperature range of 1,000–1,400 °C was investigated by neutron radiography. Hydrogen uptake can be subdivided into two steps: an initial phase and a state of equilibrium. The initial phase is controlled by the kinetics of hydrogen diffusion through the growing oxide layer. In the state of equilibrium, transport kinetics does not determine the hydrogen content of the material. An equilibrium is established between the hydrogen content of the gas environment and the metal phases. The temperature dependence of hydrogen absorption is Arrhenius-like at temperatures between 1,100 and 1,300 °C.

Keywords Steam oxidation · Zirconium alloys · Hydrogen absorption

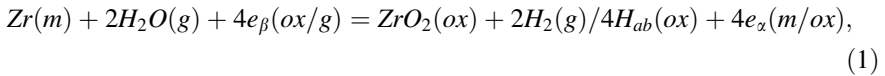
Introduction

Severe nuclear accident scenarios (accidents beyond the LOCA scenario) are studied within the QUENCH programme of the Forschungszentrum Karlsruhe. After loss of coolant, the fuel rods are overheated in steam containing, i.e. oxidizing atmosphere. Reflooding the reactor core with water as the main accident management measure enhances steam generation. The hot fuel claddings react highly exothermally with the steam in the reactor vessel. The reaction processes are

M. Grosse (✉) · M. Steinbrueck
Forschungszentrum Karlsruhe, Institut für Materialforschung I, Hermann-von-Helmholtz-Platz 1,
76344 Eggenstein-Leopoldshafen, Germany
e-mail: Mirco.Grosse@imf.fzk.de

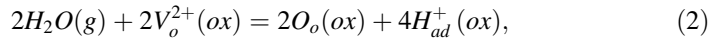
E. Lehmann · P. Vontobel
Paul Scherrer Institut Villigen, Abteilung Spallationsneutronenquelle,
5232 Villigen PSI, Switzerland

studied e.g. by [1–3]. The water molecule reacts with oxygen vacancies at the gas/oxide surface. According to [4] the resulting reaction

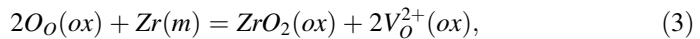


can be divided into four partial reactions:

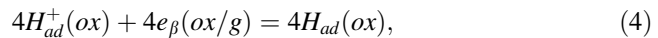
proton production/oxygen vacancy annihilation:



anodic reaction:



cathodic reaction



hydrogen release



or absorption



$\text{Zr}(m)$ represents regular zirconium atoms in the metallic phase lattice, $e_{\alpha,\beta}$ are the electrons produced by oxygen vacancy V_o^{2+} formation and the electron consumed by a proton, respectively. $H_{ad}^+(ox)$, $H_{ad}(ox)$ and $H_{ab}(ox)$ are protons or hydrogen atoms adsorbed or absorbed in the oxide, respectively. $O_o(ox)$ symbolizes an oxygen atom on a regular oxygen lattice place in the oxide.

The behaviour of hydrogen during steam oxidation of fuel rod claddings including the ratio between released and absorbed hydrogen was studied in a number of experiments [5–9]. The released hydrogen leads to the risk of hydrogen detonation. The absorbed hydrogen temporarily affects the risk of hydrogen detonation and degrades the mechanical properties of the damaged fuel rod cladding, at least at low temperatures [7]. For the Zr–Nb alloys between 10% and 40% of the hydrogen produced according to (1) were absorbed after 15 min steam oxidation at 1,000 °C depending on the niobium content and the afterwards thermal treatment [6]. In QUENCH bundle experiments, 0.8–6% of the hydrogen produced was absorbed in the residual metal [3]. In [8], it was reported that up to 70% of the hydrogen produced during steam oxidation can be absorbed by Zr–1Nb, whereas the uptake by Zry-4 is much smaller. However, the small database in [8] prevents any dependence on time of the hydrogen concentration in the zirconium alloys from being deduced. In [9], steam oxidation of Zr–1Nb was investigated. A larger data base provides more information about the dependence on time and temperature of hydrogen absorption. A nearly parabolic increase in hydrogen concentration with time is observed at 900 and 1,000 °C. The hydrogen concentration peaks at higher temperatures. The period of maximum hydrogen uptake decreases with rising temperature. The authors [9] attribute the decrease of hydrogen concentration in the later phase to the formation of the ZrO_2 layer and to reduced hydrogen solubility of the growing oxygen stabilized α -Zr(O) phase.

A theoretical description of hydrogen uptake during steam oxidation is given in [10]. As a consequence of the high oxidation rate in the beginning, hydrogen partial

pressure, p_H , in the gas phase on the sample surface is relatively high in the initial phase and low in the metal:

$$p_H^{gas} > p_H^{metal}. \quad (6)$$

Hydrogen diffuses into the metal. For this phase hydrogen concentration in the metal, $C_H^{(m)}$, increases with oxidation time, t [10]:

$$C_H^{(m)} \propto t^{\frac{3}{8}}. \quad (7)$$

The growing oxide layer between the metal and the gas phase causes the oxidation rate and, with it, hydrogen partial pressure in the gas phase, to decrease. When hydrogen partial pressure becomes higher in the metal than in the gas phase:

$$p_H^{gas} < p_H^{metal}, \quad (8)$$

hydrogen diffusion reverse out of the metal. Hydrogen is released from the metal into the gas, resulting in a decrease of $C_H^{(m)}$ with time [10]:

$$C_H^{(m)} \propto t^{-\frac{1}{8}} \quad (9)$$

The model of the initial phase was verified with the data given in [9]. However, the data-base is too small to prove the theory.

In this work, hydrogen absorption processes were studied by separate-effect tests in a furnace with well defined Ar and steam flows. The hydrogen content of steam oxidized specimens was determined at various oxidation temperatures and times by non-destructive neutron radiography [11]. The time dependence of the absorption process will be discussed below.

Material and Measurements

Measurements were carried out on Zry-4 and Duplex (Zry-4 with a 150 μm thick D4 corrosion protection layer on the outer surface) Zr–Sn cladding materials used in Western European reactor types and E110 Zr–Nb alloy used in reactors of the Russian VVER type. The chemical compositions of the alloys are listed in Table 1. The inner and outer diameters of the Zry-4 and Duplex specimens are 9.25 and 10.75 mm, respectively. The E110 specimens have an inner diameter of 7.50 mm and an outer diameter of 9.15 mm. Segments, each 20 mm long, were cut out of cladding tubes.

Figure 1 is a schematic view of the furnace in the direction of the gas flow (axial direction relative to the sample). The specimens were annealed isothermally in flowing Ar/steam atmosphere. Annealing temperatures and times varied. The test matrix is shown in Table 2. The internal structure of the furnace may give rise to gas turbulences. Mixing of the furnace gases can be assumed to occur.

Table 1 Chemical composition of the alloys investigated

Alloy	Sn	Nb	Fe	Cr	O
Zry-4	1.50	–	0.21	0.10	0.14
E110	–	0.97	<0.01	–	0.05
D4	0.50	–	0.50	0.20	0.14

Zr balance (in wt.%)

Fig. 1 Cross section of the furnace and sample holder

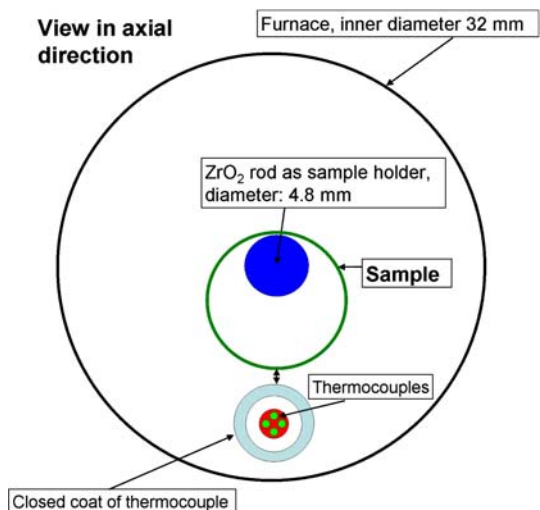


Table 2 Test matrix

Temperature in °C	1,000	1,100	1,200	1,300	1,400
Periods of oxidation in s	1,800	600	600	600	600
	3,600	1,800	1,800	1,800	1,200
	7,200	3,600	3,600	3,600	1,800
	14,400	7,200	7,200		
	21,600	14,400			

Temperature and argon and steam flows are plotted versus time in Fig. 2 as an example of a typical oxidation experiment. The specimens were moved into the furnace, which contained an Ar atmosphere at test temperature, and were held for approximately 2 min to homogenize the temperature in the sample. Steam was injected at a constant flow of 50 g/h, thus ensuring that more steam is supplied than is consumed, and steam starvation is precluded. After the end of steam injection, the specimens were kept in the furnace until the steam concentration in the off-gas decreased to approximately 2%. Then the specimens were removed from the furnace and cooled in argon atmosphere. After about 5 min, they nearly reached room temperature.

The composition of the off-gas was measured by a GAM 300 (Balzers) mass spectrometer. Figure 3 shows the hydrogen content as measured by the mass spectrometer.

To determine the hydrogen content of the cladding specimens, radiography with neutrons of a cold energy spectrum was performed at the ICON facility of SINQ/PSI [12]. The method is based on the pronounced difference between the large total macroscopic neutron cross-section, Σ_{total} , of hydrogen and the much smaller cross-sections of zirconium or zirconium oxide, ZrO₂. The radiographic image was taken with a Peltier-cooled CCD camera (type DV436 from Andor Technology, Northern

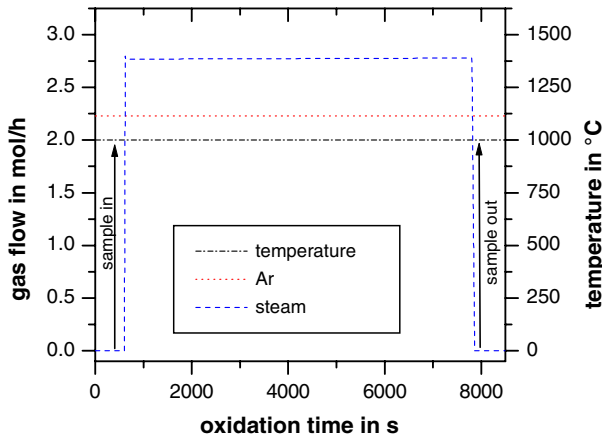


Fig. 2 Sequence of the steam oxidation tests of the material Duplex at 1000 °C for 2 h with an argon flow of 50 l/h and a steam flow of 50 g/h

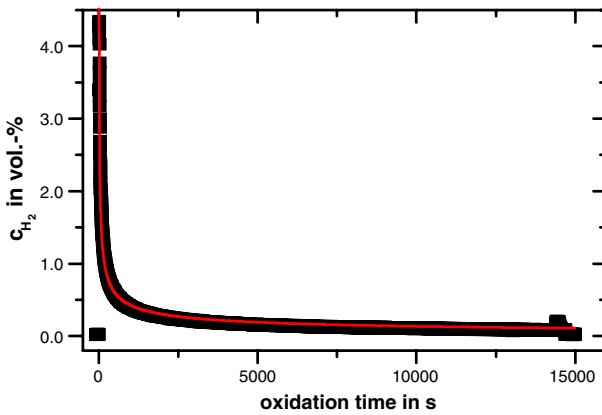


Fig. 3 Hydrogen concentration in the off-gas, c_{H_2} , during steam oxidation of Zry-4 at 1,100 °C (symbols) together with the fit $c_{H_2} \sim t^{-0.5}$ (solid line)

Ireland), combined with a Li-6-doped scintillator screen. Selected specimens were subjected to additional radiography experiments in an axial direction for which a neutron-sensitive imaging plate (BAS-ND, Fujifilm, Japan) was used. It was read out with a laser scanner (VistaScan, Duerr Dental, Germany) of 12.5 μm nominal resolution. The total macroscopic cross-sections of the oxide and the metal can be separated by these measurements. Σ_{total} was calculated from the local neutron transmission, T :

$$\Sigma_{total} = \sum_i N \sigma_{total} = \frac{-\ln(T)}{s}, \tag{10}$$

N is the number density, and σ_{total} is the microscopic cross section of the isotope, i , while s is the length of the neutron beam path through the metallic zirconium

phases. Transmission, T , is the background-corrected ratio between the neutron intensities downstream (I) and upstream (I_0) of the specimen:

$$T = \frac{I - I_B}{I_0 - I_B}, \quad (11)$$

where (I_B) is the background intensity measured behind a Cd specimen. The H/Zr atomic ratio was calculated from the total cross section with the correlation determined in [11]:

$$\frac{H}{Zr} = \frac{\Sigma_{total} - 0.21 - D_{oxide} \cdot 1.64 \cdot 10^{-4}}{2.90}, \quad (12)$$

Σ_{total} has to be in cm^{-1} , D_{oxide} is the oxide layer thickness in μm . The relative error of the determination of the total neutron cross section is better than 9%. Therefore the resolution limit for the concentration is about 1.0 at.% and the relative error of the determination of the hydrogen concentration is about 10%. A detailed description of this non-destructive method of determining hydrogen content from the attenuation of a neutron beam is given in [11].

Results

Neutron radiographic images of specimens of the three materials after steam oxidation at 1,000 °C for 2 h are shown in Fig. 4. Differences in the grey scale between the E110 specimen and the two other specimens are obvious. The different grey scales show that the hydrogen content of the E110 specimen is lower than that of the Zr–Sn specimens at this oxidation temperature and time. The horizontal intensity distributions of these measurements are indicated as well. The dependence of hydrogen concentrations in the metal phases on oxidation time as determined

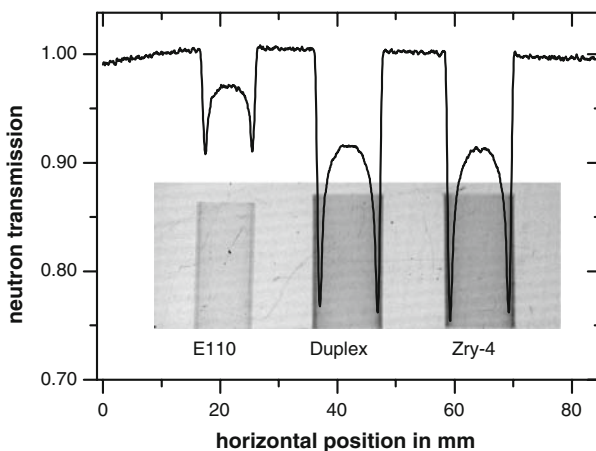


Fig. 4 Neutron radiographic image and normalized horizontal intensity distribution of specimens oxidized at 1,000 °C for 7,200 s

from the neutron radiographic data is presented in Fig. 5 for the temperatures investigated.

As shown in Fig. 5a, hydrogen uptake at 1,000 °C of the two Zr–Sn materials at different times reaches maximum H/Zr atomic ratios of approximately 10%.

In the temperature range between 1,100 and 1,400 °C shown in Fig. 5b–e, the hydrogen absorption behaviour of Zry-4 and Duplex is similar. Hydrogen concentration is nearly the same in both materials, decreasing over the time range investigated. The behaviour of the E110 Zr–Nb alloy is different at temperatures below 1,300 °C. Unlike the Zry-4 and Duplex materials, hydrogen concentration in

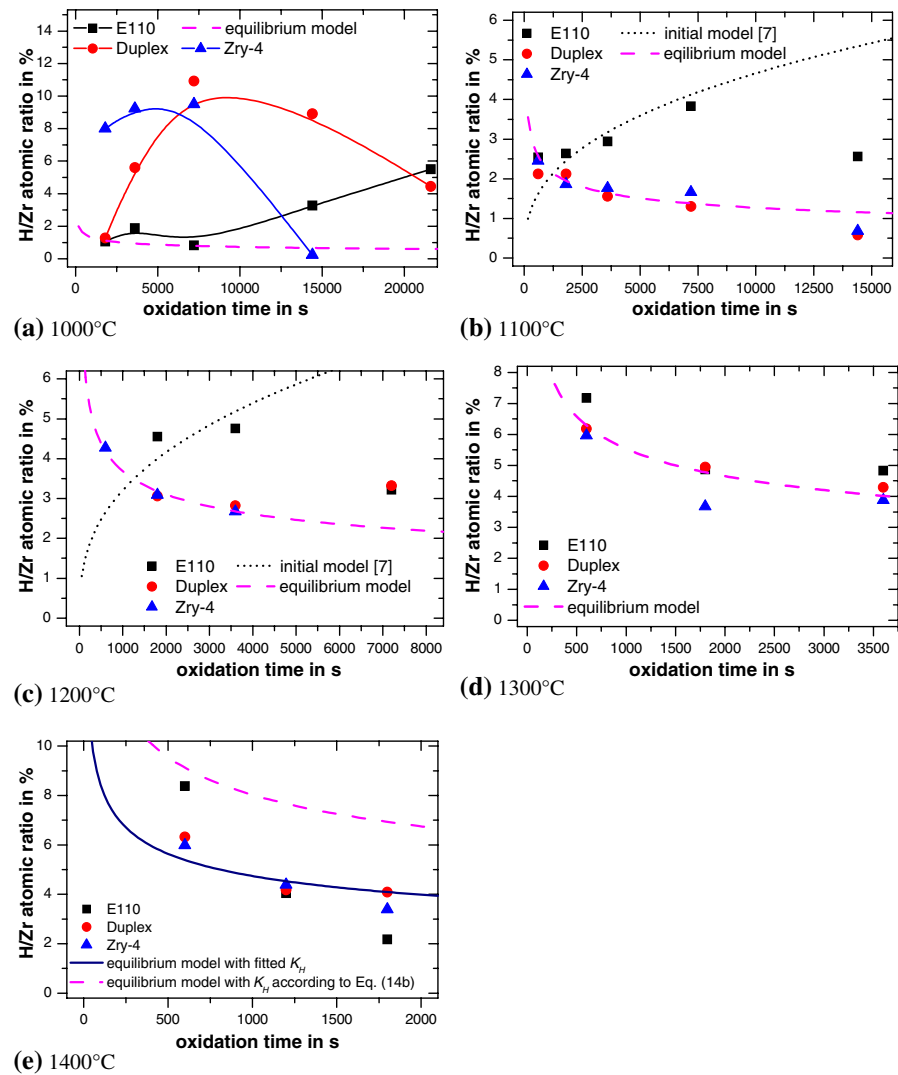


Fig. 5 Hydrogen uptake versus steam oxidation time

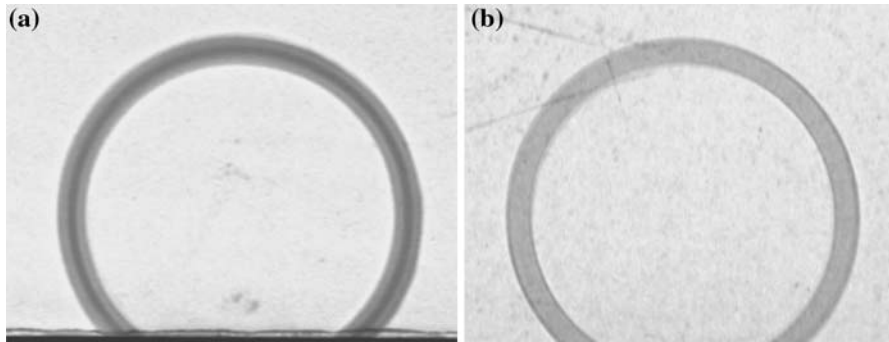
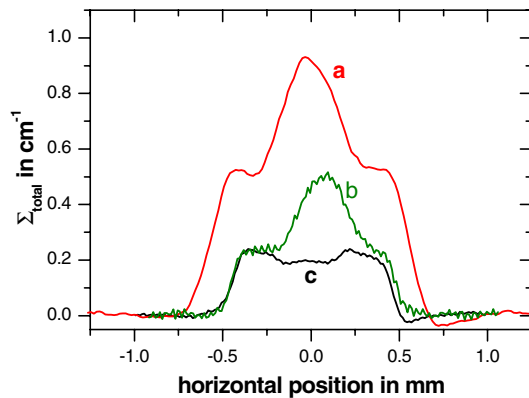


Fig. 6 Comparison of axial neutron radiographic images of Zry-4 specimens with (a) a porous oxide layer (7,200 s of steam oxidation at 1,000 °C), and (b) a hydrogen-free oxide layer (6,000 s of oxidation in O₂ at 1,200 °C)

Fig. 7 Comparison of through-wall distributions of the total neutron cross sections of a specimen with a porous oxide layer (a: Zry-4, 1,000 °C, 7,200 s, Ar/steam), a specimen with a compact oxide layer (b: Zry-4, 1,400 °C, 1,800 s, Ar/steam), and a hydrogen-free specimen (c: Zry-4, 1,200 °C, 6,000 s, Ar/O₂)



the E110 Zr–Nb alloy increases more or less at 1,000 °C throughout the time of study. At 1,100 °C and 1,200 °C, peak values are reached after 2 and 1 h, respectively. As Fig. 5d and e show, the hydrogen uptake behaviour of E110 becomes similar to that of Duplex and Zry-4 at higher temperatures.

Figure 6 is a comparison of the axial radiographic images of Zry-4 specimens, with comparable thicknesses of the oxide layers, oxidized in Ar/steam at 1,000 °C and in Ar/O₂ at 1,200 °C. Both the oxide layer and the metal exhibit stronger neutron attenuation in the steam oxidized specimen than in the hydrogen-free specimen oxidized in Ar/O₂. This effect is not found for the other materials. As Fig. 7 shows, also Zry-4 specimens oxidized at the other temperatures do not show this increase in neutron attenuation in the oxide layer.

Discussion

According to the theoretical model in [10], hydrogen uptake can be subdivided into the initial phase, with increasing hydrogen concentration, and the state of equilibrium, with decreasing hydrogen concentration in the metal.

The data for E110 oxidized at 1,100 °C fit the $t^{3/8}$ -dependence predicted in [10] for the initial phase. However, the database is too small to confirm this dependence reliably.

Hydrogen concentration in Duplex and Zry-4 oxidized at temperatures above 1,000 °C, and in E110 oxidized at 1,300 and 1,400 °C, decreases significantly faster than at $t^{-1/8}$ predicted in [10]. This discrepancy is caused by the non-laminar gas flow in the furnace. The faster decrease of hydrogen concentration in the equilibrium phase can be understood from the parabolic oxidation kinetics and the Sievert's law. In this phase a dynamic equilibrium of the hydrogen chemical activity between all phases of the system, the gas and the metal is established, independently on the kind of hydrogen species (protons, atoms or molecules) in the oxide layer. This equilibrium also does not depend on the transport mechanism through the oxide layer.

The molar amount of H_2 equals the molar amount of the total oxygen uptake, W . According to [13], a parabolic time dependence is usually assumed for this process:

$$W = K_O \cdot t^{1/2}. \quad (13)$$

On the assumption that

- hydrogen flow through the oxidation layer after the initial phase is low compared to hydrogen production,
- ideal mixing of the gases occurs in the environmental atmosphere, and
- gas flow in the environmental atmosphere is constant,

the molar oxygen uptake rate, dW/dt , reflects the true hydrogen content of the gas phase:

$$C_{H_2}^{(g)} \sim \frac{dW}{dt} = \frac{1}{2} K_O \cdot t^{-1/2} \quad (14)$$

In Fig. 3, the time dependence of the hydrogen content as measured in the off-gas and the fit according to (14) are compared for steam oxidation of Zry-4 at 1,100 °C. The good agreement validates (14). The oxygen uptake rate, K_O , depends on temperature according to the Arrhenius function:

$$K_O = A \cdot e^{\left(-\frac{Q}{RT}\right)} \text{mol s}^{-1/2}. \quad (15)$$

As the experiments were performed under normal pressure, the hydrogen partial pressure is given as:

$$p_{H_2} = C_{H_2}^{(g)} \cdot 10^5 \text{ Pa}. \quad (16)$$

According to [14], the hydrogen content in the metal phase, $C_H^{(m)}$, can be described by Sievert's law under thermodynamic equilibrium conditions for Eqs. 5a and b:

$$C_H^{(m)} = K_S \cdot p_{H_2}^{1/2}, \quad (17)$$

where K_S is the Sievert's constant, which decreases strongly with increasing absolute temperature, T :

$$K_S = \exp\left(\frac{\Delta S}{R} - \frac{\Delta H}{RT}\right) \text{Pa}^{-1/2}, \quad (18)$$

R is the molar gas constant, (8.314 J/(K mol)); ΔS , the entropy; and ΔH , the enthalpy of hydrogen solution in zirconium. The values of ΔS and ΔH depend on the oxygen content of the zirconium alloy [14]. Figure 8 shows the equilibrium hydrogen concentrations at various hydrogen partial pressures for the different zirconium phases [15].

Combining (14), (16) and (17) results in this time dependence of equilibrium hydrogen concentration in the metal to be expected for the later oxidation state (after equilibrium has been established):

$$C_H^{(m)} \sim K_S \cdot K_O^{\frac{1}{2}} \cdot t^{-\frac{1}{4}} = K_H \cdot t^{-\frac{1}{4}}, \tag{19}$$

where K_H is the rate of hydrogen uptake. Equation 19 suggests that the hydrogen content of the metal phase decreases in the equilibrium state. This conclusion means that hydrogen is no longer absorbed, but released into the environment, with zirconium acting as a hydrogen buffer.

Due to the difference of hydrogen solubilities in the α - and β -Zr phases (peaks being approximately 6 at.% for α , approximately 50 at.% for β , see Fig. 8), the temperature dependence of hydrogen uptake is determined not only by Sievert's law (17) and oxidation kinetics (13), but also by the temperature dependence of the composition of the metal phases. As is evident from Fig. 8, the α - β phase composition depends on hydrogen concentration, but also on oxygen concentration in the zirconium. Hydrogen stabilizes the β phase, while oxygen stabilizes the α phase. Consequently, an effective activation energy of hydrogen release, Q_{eff} , needs to be introduced for the temperature dependence:

$$K_H = B \cdot e^{\left(-\frac{Q_{eff}}{RT}\right)} \text{at.}\%s^{\frac{1}{4}}. \tag{20}$$

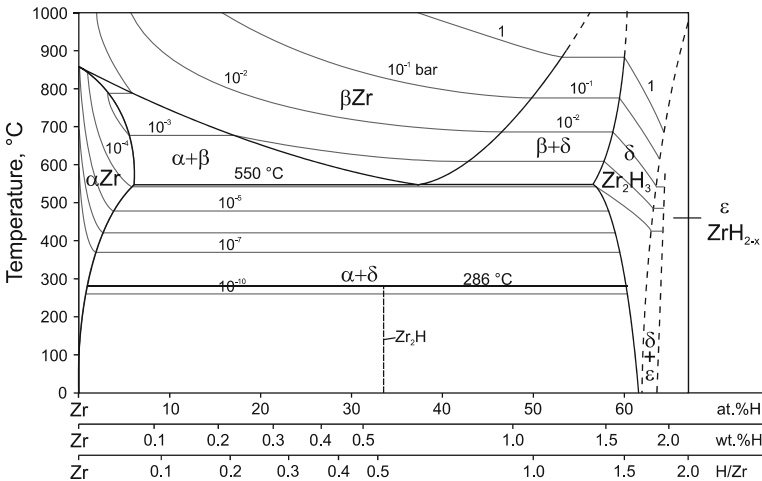


Fig. 8 Zr–H phase diagram with equilibrium concentration at various ambient hydrogen partial pressure isobars [15]

In the temperature range between 1,100 and 1,300 °C, the absorption behaviour of the two alloys Zry-4 and Duplex Zr–Sn is similar. As the broken lines in Fig. 5b–d show, hydrogen concentration of the metal fits the $t^{-1/4}$ -dependence according to (19). The dependence on the oxygen absorbed of the β – α phase composition and of hydrogen partial pressure in the β phase does not influence uptake behaviour at these temperatures. Due to the low hydrogen partial pressure of 100–400 Pa measured in the off-gas by the mass spectrometer at the end of the annealing treatment of all materials investigated, the α -Zr phase can dissolve all the hydrogen supplied (see Fig. 8). The temperature dependence of the uptake rate, K_H , between 1,100 and 1,400 °C is given in Fig. 9. Between 1,100 and 1,300 °C, it may be described by the Arrhenius-type function according to Eq. 20:

$$K_H = 14827 \cdot \exp\left(-\frac{80588 \text{ J/mol}}{RT}\right) \text{ at.}\% \text{ s}^{-1/4}, \quad (20b)$$

Q_{eff} is much higher than the value expected from the hydrogen uptake enthalpy and the activation energy of zirconium oxidation. Consequently the absorption process is dominated by the hydrogen supply from steam oxidation.

Hydrogen release behaviour at 1,000 and 1,400 °C differs from that predicted by the model. At 1,000 °C, phase transitions from tetragonal to monoclinic structures occur in the Zry-4 oxide layers. They are associated with crack formation in the oxide and spalling of part of the ZrO₂ layer, the so-called breakaway effect. The oxide layer loses at least partly its protective effect. As a result, the oxidation kinetics is rather linear than parabolic, and (13) and (14) do not apply. As the inner surface of the Duplex material is Zry-4, these processes occur also in these specimens. Hydrogen uptake in the two Zr–Sn alloys reaches local peaks at different points in time. The earlier peak of Zry-4 could be related to the breakaway effect in Zry-4 in both the outer and the inner oxide layers, but not in the protective D4 layer on the outer surface of the Duplex material. Hydrogen uptake in these two materials is much higher than predicted by Eq. 20b. Figure 10 shows metallographic images

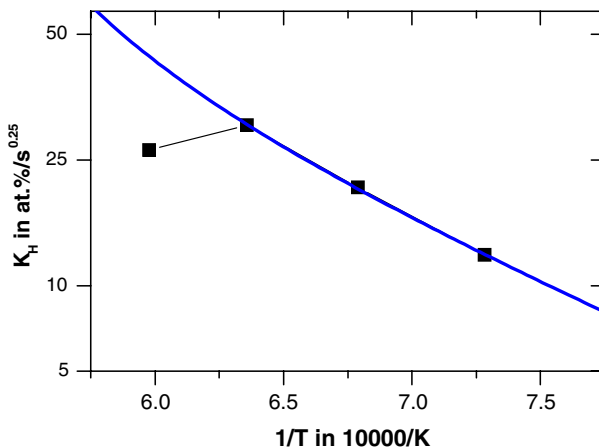


Fig. 9 Hydrogen uptake rate versus temperature

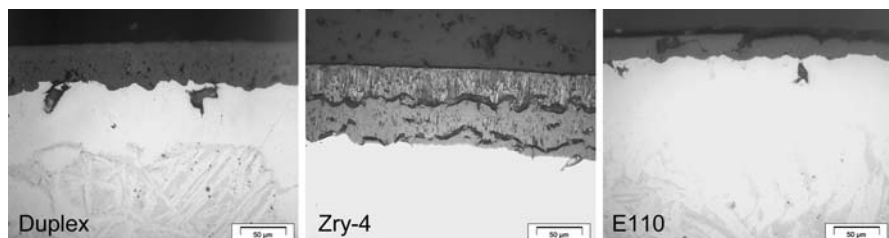


Fig. 10 Oxide layers produced after oxidation at 1,000 °C for 1 h

of the three materials investigated and oxidized at 1,000 °C for 1 h. Numerous macro and micro cracks are formed in the oxide layers of the two Zr–Sn alloys. The oxide layer in E110 is more compact, showing fewer structural failures.

Local gas flow conditions in the cracks differ greatly from global conditions. Consequently, hydrogen partial pressure is much higher in the cracks than in the off-gas as detected by the mass spectrometer. The high hydrogen content in closed cracks does not change even after annealing. As Fig. 6 shows, the total neutron cross sections of these oxide layers are significantly higher than those of compact oxide layers grown for instance at 1,400 °C.

At 1,400 °C, hydrogen partial pressure in the gas environment at the end of annealing ranges between 1.0 and 3.4 kPa, depending on the material and on oxidation time. According to Fig. 8, these hydrogen supplies are more than the α phase can absorb. On the other hand, the β -Zr phase is increasingly consumed by oxidation. In Fig. 5e, equilibrium models with fitted K_H and with K_H calculated from (20b) are compared with the experimental data. The transition from the β phase, with high hydrogen solubility, to the α phase, with lower hydrogen solubility (see Fig. 8), results in a reduction of the hydrogen content in all of the remaining metal which is more pronounced than expected from Eqs. 19 and 20. Hence, the hydrogen uptake rate deviates from the Arrhenius-type function at this temperature.

The compact oxides formed by steam oxidation at temperatures between 1,100 and 1,400 °C contain no significant amounts of hydrogen, as is shown by comparison of the total neutron cross sections of these oxide layers with the cross section of the hydrogen-free oxide layers produced by oxidation in the Ar/O₂ atmosphere (see Fig. 7).

Unlike the other two materials, niobium-alloyed E110 does not reach equilibrium at temperatures below 1,300 °C. At 1,000 °C, breakaway occurs in E110 only after long periods of oxidation (6 h). This results in an increase in hydrogen content of the metal with increasing time.

At 1,100 and 1,200 °C, peaks according to [9, 10] are found, which are attributed to the change from the diffusion-controlled initial state to the equilibrium state. The different behaviour, compared to the Zr–Sn materials, can be explained by differences in oxide morphology. In particular, the lower micro-crack density in the oxide layers of E110 results in slower hydrogen diffusion through these layers.

At 1,300 and 1,400 °C, the hydrogen absorption characteristics of E110 and the other two materials are similar. According to oxidation kinetics, hydrogen uptake in

the Zr–Nb alloy is a little higher at 1,300°C. The decrease of hydrogen content at 1,400 °C is more pronounced, as the β phase is consumed faster than in the two Zr–Sn alloys.

The time dependence is in qualitative agreement with the behaviour published in [9]. However, hydrogen concentrations of the metal as determined in the investigations presented here are significantly lower. They are accompanied by a higher oxidation rate than is found in [9]. Differences in hydrogen partial pressure in the gas caused by different gas flow rates may be the reason for this different behaviour.

Conclusions

The time dependence of hydrogen uptake during steam oxidation in the temperature range of 1,000–1,400 °C was determined by neutron radiography. Zr–Sn and Zr–Nb alloys act as hydrogen buffers in steam oxidation. Hydrogen uptake occurs only in the initial phase controlled by hydrogen diffusion through the growing oxide layer. In this phase, hydrogen uptake is proportional to $t^{3/8}$.

In the equilibrium state hydrogen release is determined by decreasing hydrogen partial pressure in the environmental gas phase. The hydrogen concentration in the metal depends on time, with $t^{-1/4}$.

The two Zr–Sn alloys investigated show similar behaviour, which differs strongly from that of a Zr–Nb alloy at temperatures below 1,300 °C. The initial phase ends, and the equilibrium phase starts much earlier for Zry-4 and Duplex than for E110. At 1,100 °C, it only takes minutes for equilibrium to be established in the Zr–Sn alloys, but approximately 2 h in the Zr–Nb alloy.

At 1,000 °C, the breakaway effect observed in the oxide layer of all materials results in high hydrogen uptake. Hydrogen is also stored in the porous oxide layer.

At higher temperatures, Zry-4 and Duplex show the behaviour of the equilibrium state after a short time. The temperature dependence is Arrhenius-like. Hydrogen content in the metallic phases depends on the α – β phase composition only for an oxidation temperature of 1,400 °C.

Acknowledgements This work is based on experiments performed at the ICON facility of the Swiss Spallation Neutron Source SINQ, Paul Scherrer Institute, Villigen, Switzerland. The authors are grateful to G. Frei, G. Necola, and G. Kühne of PSI-ASQ for their support during the radiography experiments, and to U. Stegmaier and P. Severloh of FZK-IMF1 for the metallographic investigations. The authors also thank Prof. M. Veshchunov of the IBRAE Institute Moscow for fruitful discussions.

References

1. L. Sepold, P. Hofmann, W. Leiling, A. Miassoedov, D. Piel, L. Schmidt, and M. Steinbrück, *Nuclear Engineering and Design* **204**, 205 (2001).
2. M. Steinbrück, *Proceedings of the 13th International QUENCH Workshop* (Forschungszentrum Karlsruhe, November 20–22, 2007), ISBN 978-3-923704-63-7.
3. L. K. Sepold, A. Miassoedov, G. Schanz, U. Stegmaier, M. Steinbrueck, and J. Stuckert, *Nuclear Technology* **147**, 202 (2004).

4. C. Wagner, *Berichte d. Bunsen-Gesellschaft f. Physikalische Chemie* **72**, 778 (1968).
5. K. Park and D. R. Olander, *Journal of the American Ceramic Society* **74**, 72 (1991).
6. K.-N. Choo, S.-I. Puyn, and Y.-S. Kim, *Journal of Nuclear Materials* **226**, 9 (1995).
7. J. H. Kim, M. H. Lee, B. K. Choi, and Y. H. Jeong, *Journal of Nuclear Materials* **235**, 67 (2005).
8. J. Böhmert, M. Dietrich, and J. Linek, *Nuclear Engineering and Design* **147**, 53 (1993).
9. J. Freska, G. Konczos, L. Maroti, and L. Matus, Oxidation and hydration of Zr 1% Nb alloys by steam, KFKI-Report-1995-17/G (1995).
10. M. S. Veshchunov and A. V. Berdyshev, *Journal of Nuclear Materials* **255**, 250 (1998).
11. M. Grosse, E. Lehmann, P. Vontobel, and M. Steinbrueck, *Nuclear Instruments & Methods in Physics Research A* **566**, 739 (2006).
12. G. Kühne, G. Frei, E. Lehmann, and P. Vontobel, *Nuclear Instruments & Methods in Physics Research Section A* **542**, 264 (2005).
13. G. Schanz, B. Adroguer, and A. Volchek, *Nuclear Engineering and Design* **232**, 75 (2004).
14. M. Steinbrück, *Journal of Nuclear Materials* **334**, 58 (2004).
15. M. Steinbrück and H. Kleykamp, unpublished.